Technical University of Denmark

**DTU**

# Increased Mass Loss and Asynchronous Behavior of Marine-Terminating Outlet Glaciers at Upernavik Isstrøm, NW Greenland

**Larsen, Signe Hillerup; Khan, Shfaqat Abbas; Ahlstrøm, Andreas Peter; Hvidberg, Christine Schøtt; Willis, Michael John; Andersen, Signe Bech**

**DTU Library**
Technical Information Center of Denmark

**Key Points:**
- Reaction of ice stream flow to climate change is dependent on glacier geometry
- Acceleration of Upernavik Ice stream, NW Greenland, since 2005

**Correspondence to:**
S. H. Larsen,
shl@geus.dk

# Increased mass loss and asynchronous behavior of marine-terminating outlet glaciers at Upernavik Isstrøm, NW Greenland

Signe Hillerup Larsen[1,2], Shfaqat Abbas Khan[3], Andreas Peter Ahlstrøm[1], Christine Schøtt Hvidberg[2], Michael John Willis[4,5], and Signe Bech Andersen[1]

[1]Department of Marine Geology and Glaciology, Geological Survey of Denmark and Greenland, Copenhagen, Denmark, [2]Centre for Ice and Climate, Niels Bohr Institute, University of Copenhagen, Copenhagen, Denmark, [3]Department of Geodesy, DTU Space-National Space Institute, Technical University of Denmark, Kongens Lyngby, Denmark, [4]Department of Earth and Atmospheric Sciences, Cornell University, Ithaca, New York, USA, [5]Department of Geological Sciences, University of North Carolina at Chapel Hill, Chapel Hill, North Carolina, USA

**Abstract** In order to model and predict future behavior of marine terminating glaciers, it is essential to understand the different factors that control a glaciers response to climate change. Here we present a detailed study of the asynchronous changes in dynamic behavior of four adjacent marine-terminating glaciers at Upernavik Isstrøm (UI), northwest Greenland, between 1992 and 2013. Velocities were stable for all outlets at UI between 1992 and 2005. The northernmost glacier started to accelerate and thin in 2006 and continued to do so into 2011 after which time the velocities stabilized. The second most northerly glacier started to accelerate and thin in 2009 and continued to do so until the last observations in 2013, dramatically increasing the area affected by dynamically induced thinning. The southern glaciers show little change, with the most southerly glacier undergoing slight retreat and deceleration between 1992 and 2013. These observations point out the fact that the UI glaciers are reacting to climate change on different timescales. The asynchronous behavior of the four neighboring glaciers is explained in terms of the individual glaciers geometry and terminus position. The northernmost glacier is believed to have had a floating tongue between 1985 and 2007 which disintegrated in 2007–2008. This release of back stress destabilized the glacier causing it to accelerate and thin rapidly. We suggest that the ice tongue broke up due to ocean-warming-induced thinning in the late 1990s. Recent response on UI glaciers is found to be related to increased surface melt. Our investigations suggest that three out of the four main glaciers in the UI are likely to be in unstable positions and may have the potential to rapidly thin and accelerate and increase their contribution to sea level in the future.

## 1. Introduction

The mass loss rate of the Greenland ice sheet doubled from about 150 Gt yr$^{-1}$ between 2000 and 2005 to more than 300 Gt yr$^{-1}$ between 2009 and 2012 [*Enderlin et al.*, 2014; *Khan et al.*, 2014a; *Helm et al.*, 2014]. Of the mass loss between 2000 and 2012, 30–50% was through ice discharge in the form of calving at marine-terminating glaciers [*Enderlin et al.*, 2014; *Khan et al.*, 2015; *van den Broeke et al.*, 2009]. Marine-terminating glaciers show nonlinear reactions to external forcings such as warming of ocean and air temperatures as well as differences in bed geometry as the grounding line advances and retreats [*Nick et al.*, 2009; *Schoof*, 2007; *Meier and Post*, 1987]. Neighboring glaciers can therefore react quite differently to similar climate forcings as observed by *Khan et al.* [2013] at Upernavik Isstrøm (UI) in NW Greenland. UI consists of several fast flowing ice streams that terminate into the same fjord (Upernavik Isfjord) (Figure 1) and is therefore an optimal study site for examining the interaction between climate, ice dynamics, bedrock topography, and the influence of the ocean. UI was first observed in 1849 when it terminated in a single glacier trunk [*Weidick*, 1958] and has since retreated by 25–30 km and split into several glaciers.

In this paper we present a detailed study of the asynchronous changes of four marine-terminating outlet glaciers at UI. We focus on the four main east to west flowing glaciers which we number UI-1 to UI-4 from north to south, respectively (Figure 1). The study by *Khan et al.* [2013] provided evidence of two instances of
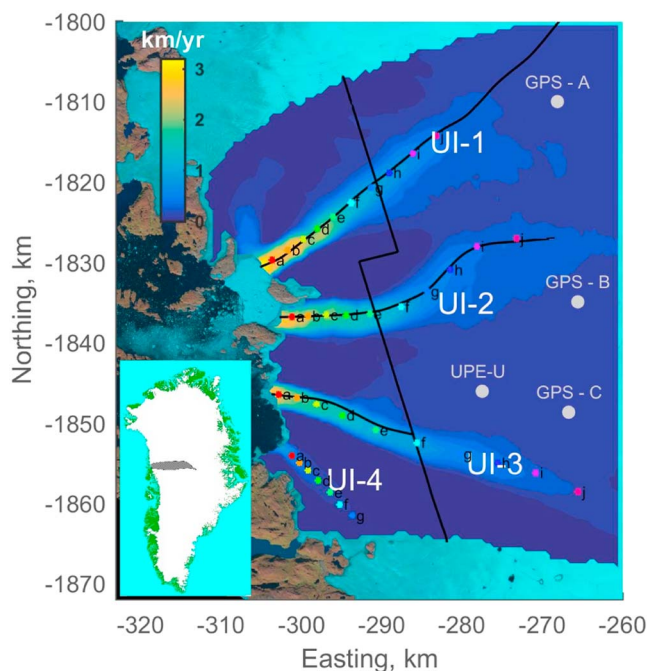
**Figure 1.** Velocity map of UI winter velocities 2000/2001 [*Joughin et al.*, 2010] for the lower part of the UI catchment. Black north/south ward lines indicate Center for Remote Sensing of Ice Sheets (CReSIS) crossing lines, 2010 [*Gogineni*, 2012], used as fluxgate. Black center lines of each glacier is the CReSIS lines from 2013 [*Gogineni*, 2012] used in Figure 2. Colored points marked a–j on each glacier mark the points along the center line where velocities are plotted in Figures 9 and 10. The dots indicate the position of the Programme for Monitoring the Greenland Ice Sheet (PROMICE) automatic weather station UPE-U (966 m above sea level), and the position of the three permanent GPS stations used for elevation change studies. Landsat image (available from the U.S. Geological Survey) from 2000 is used as background. Inserted is Greenland ice/land mask [*Citterio and Ahlstrøm*, 2013]; the shaded area indicates the catchment area of UI. Easting and northing are in polar stereographic projection using 45°W and 70°N as reference.

increased dynamically induced thinning at UI outlet glaciers. The first event occurred on the southernmost tributary (UI-4) between 1985 and 1991, while the second occurred on the northernmost tributary (UI-1) between 2005 and 2010. Both events occurred during periods when both air and ocean temperatures were observed to be anomalously high and the dynamic changes were suggested to be triggered by this according to *Khan et al.* [2013]. However, the outlets of UI are, due to their proximity, considered to be subject to similar external forcing, from changes in the surface air temperature and precipitation as well as from changes in the ocean temperature. The different reactions to similar forcings must therefore be due to differences in the nonlinear response to climate change of the individual UI outlet glaciers.

We aim to examine the asynchronous behavior of the four neighboring outlet glaciers and establish if it is likely that the glaciers will show continued increase in dynamic mass loss, providing a record for calibration and validation of future ice dynamic modeling experiments. To do this, we provide an extended analysis (compared to that of *Khan et al.* [2013]) of changes in velocity, terminus position, and surface elevation to show the detailed dynamic behavior of the UI outlets. We also examine the changes in regional climate model data of surface mass balance (SMB) and the different bedrock geometry of each of the UI glaciers. From this we are able to establish how differences in terminus position, bed, and fjord geometry can cause different nonlinear response of the glaciers.

We first present the geometry of the UI outlets from existing airborne radar data along the center lines of the glaciers [*Gogineni*, 2012] and then examine the sparse bathymetry of the fjord. We then present recent changes in SMB, calving front position, and surface elevation and compare them to the changes in ice velocities. The velocity data are also used in a simple flux gate calculation to give an estimate of the increase in mass loss between 2000 and 2012 partitioned into surface melt and ice discharge. Finally, the observations are discussed in terms of each individual glaciers' sensitivity to changes in climate forcing.
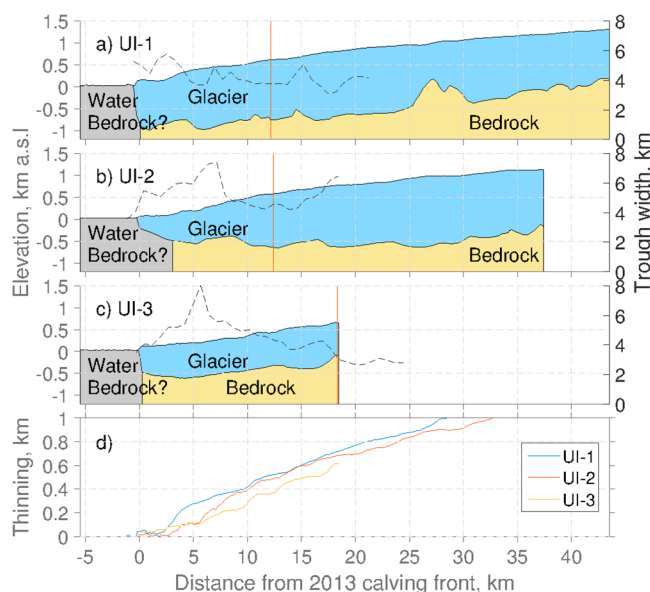
**Figure 2.** (a–c) Surface and bed topography of glaciers UI-1 to UI-3 from CReSIS level 2 radar depth data [*Gogineni*, 2012] obtained 18 April 2013. Light blue indicates glacier ice, yellow indicates bedrock, and gray indicates fjord water or bedrock. The bedrock in the fjord is unknown due to the impenetrability of radar through water. The vertical orange line indicates the position of the fluxgate. UI-4 is not shown due to lack of good data. The dashed black line shows the glacier trough width measured every 750 m along the center flow line of each glacier. (d) Thinning required to reach buoyancy based on the data in Figures 2a–2c, assuming that the entire glacier is pure ice, with density $\rho_{ice} = 917$ kg m$^{-3}$.

## 2. Environmental Settings

The stability of glaciers and ice streams have been shown to be related to the bedrock geometry beneath the glacier. The slope of the bed of a glacier and the width of the glacier trough both influence the dynamics of a glacier [e.g., *Carr et al.*, 2013; *Khan et al.*, 2014b; *Enderlin et al.*, 2013]. If a glacier moves into deeper water or a wider fjord, the calving front area increases, which can increase the calving rate [*Schoof*, 2007]. A fjord widening will, furthermore, cause divergence of the flow which will cause thinning of the glacier, reducing the relative lateral shear stress. In addition, a glacier with a floating tongue is likely to be more sensitive to ocean temperatures due to the higher surface area in contact with ocean waters compared to a grounded calving front [*Straneo et al.*, 2013]. Measurements of bed geometry and fjord bathymetry are therefore crucial for understanding the glacier system as a whole.

The surface and bed of the center lines of the four glaciers were measured directly with radar in 2013 by the Center for Remote Sensing of Ice Sheets (CReSIS) [*Gogineni*, 2012] (Figure 2). From the radar data the calving front of UI-1 is observed to be 1 km in thickness and grounded in 2013. The bedrock elevation gradually rises inland up to around sea level at a distance of about 45 km from the front. The inferred basal topography from *Morlighem et al.* [2014] suggests that the glacier trough is narrow but widens only a few kilometers inland from the 2013 front position (Figures 2a and 3). The front of the second glacier, UI-2, is about 250 m thick according to radar data (Figure 2). The surface slope decreases toward the front, and the surface of the outermost 2–3 km of the glacier is horizontal. Although the quality of radar data decreases close to the calving front, the data indicate that UI-2 has a floating ice tongue of around 2.5 km in length. This is supported by the surface elevation being at buoyancy (Figure 2d). The elevation change observed between 2011 and 2014, using high-resolution (3 m) digital elevation models (Figure 4) show low-elevation change at the southern part of the frontal area of UI-2 compared to the northern part, indicating that this area of the glacier could be afloat. Landsat images from, e.g., 14 June 2009 and 17 June 2010, show large tabular icebergs (~500 m in diameter) floating away from the front, supporting this interpretation. UI-2 has a downward sloping bed up to 25 km inland from the grounding line, and the inferred basal topography (Figures 2b and 3) shows the trough getting wider until about 7 km inland. The calving front of the third glacier, UI-3, is about 500 m thick according to radar data (Figure 2). The surface slope is steadily decreasing toward the margin, and base is horizontal, suggesting that it is grounded. The bed is slightly downward sloping inland, and the trough of UI-3 is by far the longest of the four glaciers and found to be below sea level for up to 142 km inland [*Morlighem et al.*, 2014].
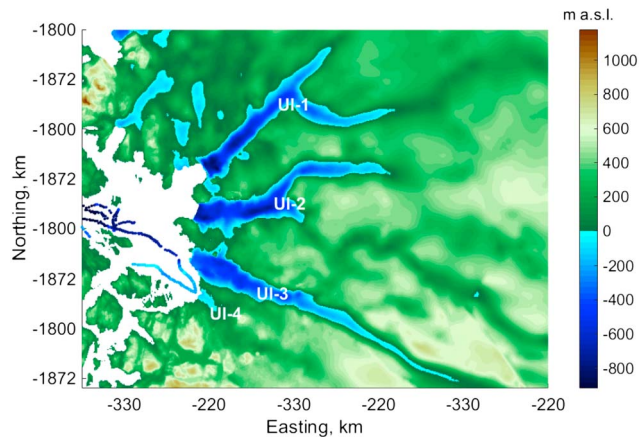
**Figure 3.** Inferred basal topography from *Morlighem et al.* [2014] and bathymetry data from *Andresen et al.* [2014]. Easting and northing are in polar stereographic projection using 45°W and 70°N as reference.

The trough of UI-3 widens until about 5 km inland (Figure 2c), and the first 5 km has ice thicknesses that are within 100 m from being floating. For the fourth glacier, UI-4, the radar depth data have many data gaps, and the profile is therefore not shown. The inferred basal topography (Figure 3) suggests that the base of UI-4 is less than 200 m below sea level at the front and that the bedrock is above sea level about 5 km from the front [*Morlighem et al.*, 2014]. This suggests that UI-4 is shallow with ice thicknesses below 400 m between the front and 5 km inland.

The fjord bathymetry is important for fjord water circulation and for which water masses are able to reach the glacier margin [*Straneo and Heimbach*, 2013]. Furthermore, it gives an indication of the glacier bed in the
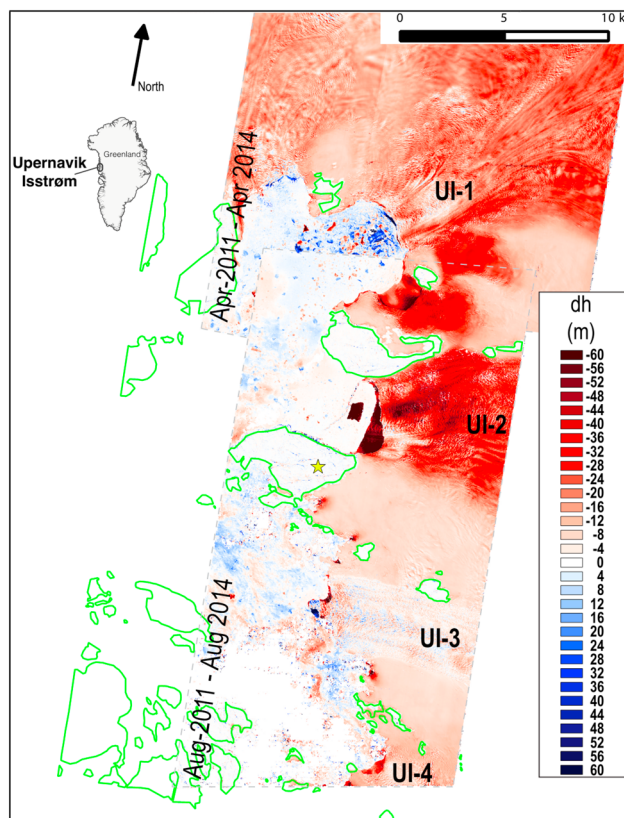


**Figure 4.** The elevation change between 2011 and 2014 from high-resolution (3 m) digital elevation models.
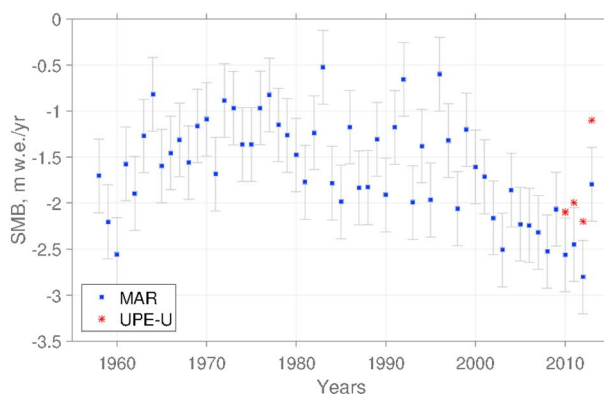
**Figure 5.** Blue, average SMB from the regional climate model MAR (Modéle Atmosphérique Régional) [*Fettweis et al.*, 2013] for the years 1958–2013. MAR SMB is averaged over the area downstream of the fluxgate (see Figure 1). Red, point measurements of net SMB from the PROMICE automatic weather station UPE-U for 2009–2012.

past at former, more advanced positions of the front. Bathymetry measurements from *Andresen et al.* [2014] (Figure 3) show water depths of around 1 km in most of the fjord. Due to ice conditions, it is not possible to measure water depths near the front of glacier UI-1 and UI-2. The glacier trough is inferred to be more than 900 m deep at the terminus of UI-1 (Figures 2 and 3), and so the inner parts of the fjord in front of UI-1 and UI-2 are also expected to be around this depth (Figure 3), but the presence of sills cannot be excluded. The water depth in front of UI-3 is below 900 m according to the bathymetry measurements by *Andresen et al.* [2014] (Figure 3). The southern part of the fjord, where UI-4 terminates, is shallower, and only about 200 m deep close to the front of UI-4 [*Andresen et al.*, 2014]. Warm subsurface ocean water, which is observed to occur at a depth below 200 m, can therefore reach UI-1 to UI-3 whereas UI-4 is more likely to be only affected by cold polar waters [*Andresen et al.*, 2014].

## 3. Recent Changes

As reported by *Khan et al.* [2013] and *Nielsen et al.* [2012], major acceleration, thinning, and retreat have been observed, mainly at UI-1, between 2000 and 2010. Here we extend the observation record and show changes in surface climate and calving front position and compare this with velocity and surface elevation changes until 2013. We further analyze velocity changes by investigating seasonal changes in velocity from 2009 to 2013.

### 3.1. Surface Mass Balance

SMB data since 1958 (Figure 5) are provided as output from the regional climate model, MAR v3.5 (Modéle Atmosphérique Régional) [*Fettweis et al.*, 2013]. The most important finding is that SMB values are generally more negative during the last decade compared to the previous four decades. The SMB from MAR is averaged over the lower ablation area (downstream of the flux gate as indicated by black lines in Figure 1) and compared with the point measurement of SMB from an automatic weather station (UPE-U) operated by the Programme for Monitoring the Greenland Ice Sheet (PROMICE) (see location in Figure 1). The variations in SMB agree between the two data sets for the overlapping period between 2009 and 2012. The PROMICE data show higher values mainly due to the location of the weather station at a higher elevation than the area over which SMB from MAR is averaged.

### 3.2. Calving Front Position

Calving front positions are mapped from Landsat 7 and Landsat 8 images (Figure 6). To obtain a record from the time of annual minimum ice extent, the latest cloud-free image from August or September is used for each year. Years with no useful Landsat images in August and September are discarded. All glaciers exhibit an overall retreat during the period 1985–2013. The retreat of UI-1 leads the calving front into a wider fjord and the northern tributary of UI-1 detached from the main glacier around 2006. This is followed by a major (4 km) retreat of UI-1 between 2007 and 2008. Due to the very rapid retreat, and the observation of large tabular icebergs floating away (as seen on Landsat images from, e.g., 4 April 2007 and 8 May 2008),
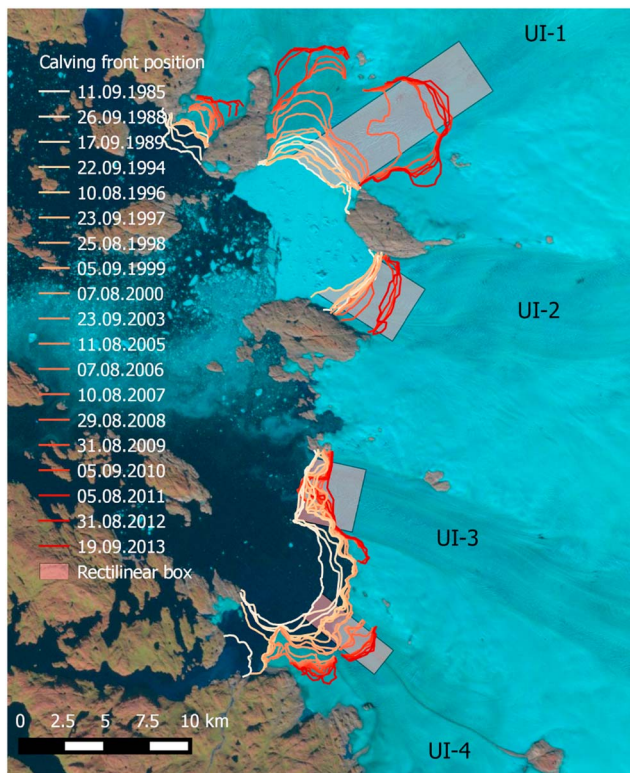
**Figure 6.** Calving front position from Landsat images. The calving fronts are digitized from the last available image from each year, usually around August–September. The colored boxes indicated the rectilinear boxes used for obtaining calving front retreat in Figures 7 and 8.

this is interpreted as the disintegration of a floating ice tongue. The calving front retreat is investigated in more detail in Figures 7 and 8 where the retreat is defined using the rectilinear box method [e.g., *Moon and Joughin*, 2008; *Carr et al.*, 2013; *Lea et al.*, 2014]. A rectilinear box is defined over the glacier front (Figure 6), and the retreat is then calculated as the area change of the box covering the glacier, divided by the width of the box. By using this method, we are able to account for the asymmetric retreat of the calving fronts. However, mapping the calving front of UI-3 posed a problem as it appears that icebergs are grounded on a topographical



**Figure 7.** The distance from the 1985 calving front position using the rectilinear box method; boxes are shown in Figure 6.

**Figure 8.** The retreat of the calving front since last measurement, using the rectilinear box method; boxes are shown in Figure 6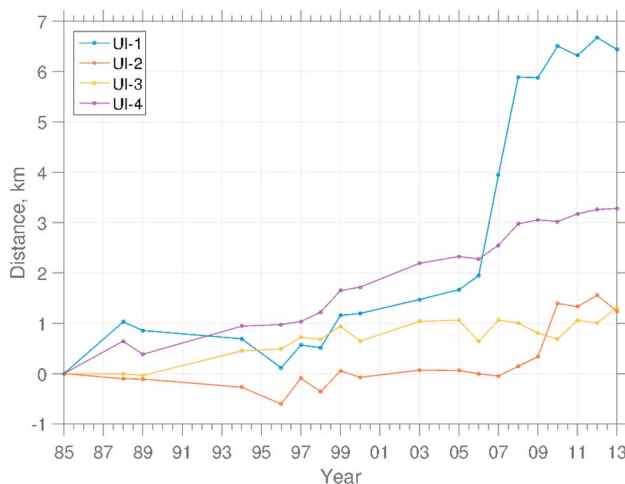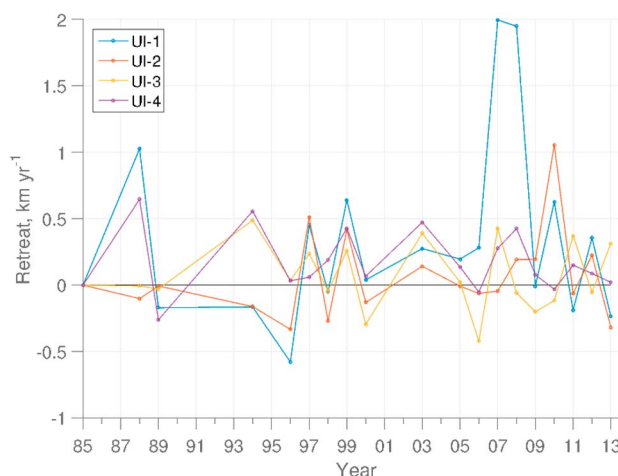. The retreat is divided by the number of years between measurements, so the units are in km yr$^{-1}$. Positive values indicate that the calving front is further inland than the previous year, and negative values indicate an advance of the calving front.

high point just at the center of the calving front. In some years icebergs were not clearly detached from the glacier and are therefore mapped as part of the glacier (see Figure 6). Thus, the measured calving front fluctuations are not necessarily representative of the calving front behavior.

All of the glaciers exhibited an overall retreat during the 28 year period studied here. The retreat of UI-1 started around 1997, and rates peaked in 2007 and 2008 after which the retreat rate slowed to previous levels, but the retreat continued through 2012. UI-2 showed fluctuations of $\pm 500$ m in the calving front position during 1997–1999 (Figure 8). The glacier retreated rapidly by 1.5 km between 2008 and 2010 after which the calving front remained stable. UI-3 showed fluctuations in calving front position but only a slight retreat of 1.2 km since 1985, and the calving front of UI-4 showed a general retreat between 1985 and 2013 in which period the front retreated 3.3 km (Figure 7).

### 3.3. Ice Flow Velocity

Figure 6 shows winter velocities between the winter of 1992/1993 and the winter of 2013/2014. For the years 1992/1993 to 1996/1997 and again 2002/2003 to 2004/2005 velocity data are from *The ESA Climate Change Initiative - Ice Sheets, program for Greenland* [2015]. For the period 2000/2001 and 2005/2006 to 2013/2014 velocity maps from *Joughin et al.* [2010, 2011] are used. From 1992 to 2005 the glaciers were flowing with similar and constant speeds. The asynchronous acceleration of the individual glaciers in the subsequent years is described below.

The speed near the terminus of UI-1 (Figure 9a, points a–d) increased by about 50–60% (2 km yr$^{-1}$) between 2006 and 2008 in response to the disintegration of the floating ice tongue (Figure 6). Acceleration reached at least 20 km inland, with a speed increase of around 25% (500 m yr$^{-1}$) at points h–j. Between 2009 and 2010 UI-1 decelerated by about 15% (1 km yr$^{-1}$) near the terminus (point c) and remained stable further inland (points d and e), before it resumed acceleration and reached its maximum observed speed in 2011 (5 km yr$^{-1}$ at point c); in 2012–2013 the ice flow speeds remained at this high level. UI-2 started to accelerate after 2008, and at point a, the flow speed gradually increased by around 300 m yr$^{-1}$ each year up until the last observation in 2013 (Figure 9b). In total, the gradual velocity increase is of around 50% (1.5 km yr$^{-1}$) since 2008 near the terminus and 15% (200–300 m yr$^{-1}$) about 20 km inland. UI-3 showed a slight decrease in ice flow speed (Figure 9c) (1–2% or 100–200 m yr$^{-1}$ at points a and b) between 2000 and 2013. UI-4 showed a general decrease in flow speeds over the period with the exception of 2009–2010 when velocities increased by about 30–40% near the terminus (points a and b). After 2008 the glacier decelerated and returned to the background velocity.

Seasonal velocity patterns of marine-terminating glaciers around the coast of Greenland were studied by *Moon et al.* [2014] and from velocity measurements between 2009 and 2013, glaciers were classified within three types. Type 1 glaciers are glaciers where the seasonal speedup correlates well with the terminus
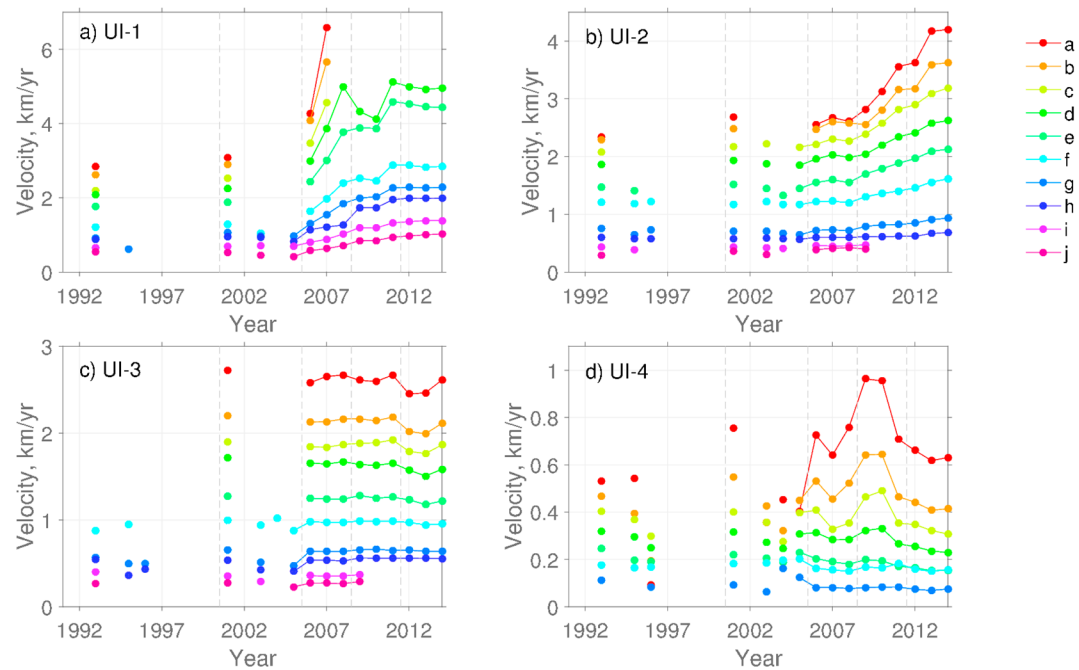
**Figure 9.** Winter velocities (data from *Joughin et al.* [2010] and *The ESA Climate Change Initiative - Ice Sheets, program for Greenland* [2015]) at points denoted a–j and marked with colored points in Figure 1, along the flow lines of UI-1 to UI-4. Point a is closest to the calving front for each glacier. The dashed vertical lines show the three time intervals used in Tables 1 and 2. Flow is fastest at the calving front of all glaciers, decreasing with distance upstream.

position and are therefore primarily controlled by ice front position. Types 2 and 3 are glaciers where the seasonal velocity patterns are primarily correlated with meltwater runoff. Type 2 glaciers have a strong early summer speed increase, with a slowdown to winter speeds that occurs near midsummer indicating that the glacier bed is lubricated by meltwater reaching the bed. Type 3 glaciers have a late spring/early summer speedup and a late summer minimum where ice flow speeds are lower than winter velocities. This could indicate that there is enough meltwater available at the glacier bed for the subglacial hydrological system to become so efficient that all basal water is removed from the bed through large channels and the glacier bed is therefore less slippery. The glaciers UI-1, UI-2, and UI-3 were included in the study by *Moon et al.* [2014], and while UI-1 and UI-2 did not show any distinct patterns during 2009–2013, UI-3 showed type 2 behavior. Figure 10 shows the velocities 4–5 times per year, along the same profiles as in Figure 9, with the melt season highlighted in gray. All glaciers exhibited spring or summer speedup and while UI-1 and UI-2 showed variation in when and by how much the slowdown occurred, UI-3 showed type 2 behavior, confirming the description in *Moon et al.* [2014]. UI-4 can be categorized as a type 3 glacier with early spring speedup and midsummer slowdown below winter speeds. This could indicate that an efficient drainage system can develop during the melt season at UI-4. For every melt season UI-4 decelerated to velocities lower than previous years resulting in a general deceleration between 2009 and 2013. From Figure 9a we see that the acceleration event at UI-1 in 2010 was a short-duration event that occurred between July and August. In contrast, the acceleration of UI-2 was nearly constant throughout the 2008–2013 period (Figure 10b), highlighting the difference between the two glaciers' behavior.

### 3.4. Ice Surface Elevation

Surface elevation changes were highly variable between 2005 and 2011 for the lower parts of the UI ablation area [*Nielsen et al.*, 2012]. To get a better idea of the spatial and temporal changes between 2008 and 2012, we use lidar elevations collected by the Airborne Topographic Mapper (ATM) [*Krabill*, 2013]. Since the ATM lines do not repeat the same track every year, we use a SPOT 5 HRS digital elevation model (DEM) from 3 June 2008 [*Korona et al.*, 2009] as a reference DEM and evaluate elevation changes relative to this. The SPOT DEM is the same as used in *Nielsen et al.* [2012], has a resolution of $40 \times 40$ m, and is corrected for a constant bias in elevation according to *Nielsen et al.* [2012] (Figure 11). In 2008 and 2009, major thinning of $15-20$ m yr$^{-1}$ was observed on UI-1, followed in 2010 or 2011 by thinning of around $20-30$ m yr$^{-1}$ at UI-2, both continued
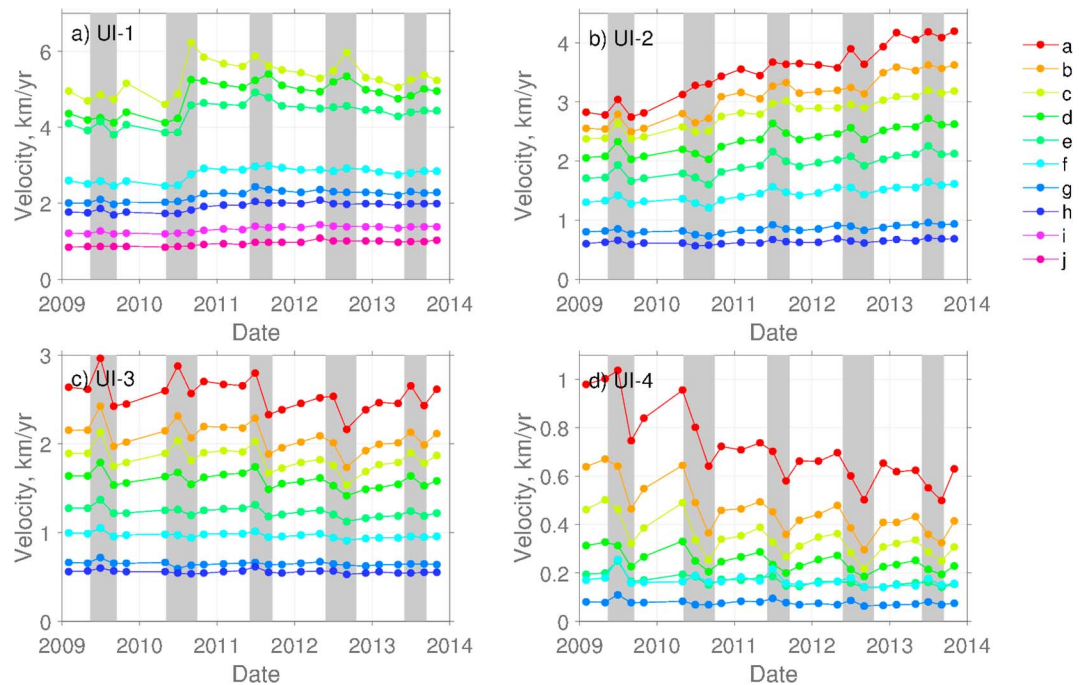
**Figure 10.** Monthly velocities for mainly February, April, July, August, and November between 2009 and 2013, at points denoted a–j and marked with colored points in Figure 1, along the center flow lines of UI-1 to UI-4 (2009–2011 data from *Joughin et al.* [2011]; 2012–2013 data from S. H. L. Joughin (personal communication, 2015)). The shaded areas indicate the periods with average daily temperatures above melting point at the PROMICE weather station UPE-L.

to thin into 2012. While UI-1 and UI-2 thinned up to 80 m between 2008 and 2013, UI-3 showed a total surface lowering below 10 m and UI-4 a 10–20 m total elevation lowering (Figure 11). The measured elevation and the thinning rates at three permanent GPS stations located on ice 30–40 km upstream (see location in Figure 1) are shown in Figure 12. At GPS-A the thinning rates changed around 2005 from 0.2 m yr$^{-1}$ to 1.3 m yr$^{-1}$ and then again around 2010 to 2.3 m yr$^{-1}$. For GPS-B the thinning rate changed around 2010 from 0.5 m yr$^{-1}$ to 1.7 m yr$^{-1}$, and for GPS-C the thinning rate remained constant around 1.1 m yr$^{-1}$. SMB rates modeled by MAR indicate that surface melt rates were much smaller than the observed thinning rates at each of the GPS points. This suggest that the dynamically induced thinning of both UI-1 and UI-2 has propagated at least 40 km upstream. GPS-C is located approximately 25 km from the margin and 10 km north of UI-3, and there-fore, it may be affected by dynamic thinning propagating from UI-2 or UI-3. From Figures 4 and 11 it is clear that UI-3 experienced only little thinning below 10 m between 2008 and 2013. The observed thinning at GPS-C exceeded the surface mass balance (Figure 12), and it is thus likely that dynamic thinning from UI-2 has propagated to the location of GPS-C (Figure 11).

### 3.5. Total and Partitioned Increase in Mass Loss Since 2000

To establish how closely changes in SMB and ice discharge are linked, we calculate the individual components of the increase in mass loss since 2000.

The total increased mass loss since 2000 ($\Delta$MB) is the sum of the contribution from surface melt ($\Delta$SMB) and ice discharge ($\Delta D$), expressed as

$$\Delta MB = \Delta D + \Delta SMB \qquad (1)$$

To understand the relative magnitude of the increase in dynamic mass loss, $\Delta D$, compared to the total mass balance anomaly ($\Delta$MB), we need to close the mass balance budget.

The increase in ice discharge since 2000, $\Delta D$, is calculated for the UI catchment (see insert in Figure 1) using a simple flux gate calculation. The flux gate is about 10 km upstream from the grounding line, following two CReSIS radar lines from 2010 that crossed the UI ice streams (Figure 1). $\Delta D$ is mainly given by the change in flux through the fluxgate, $\Delta F$. However, to account for the dynamic mass loss between the fluxgate and the
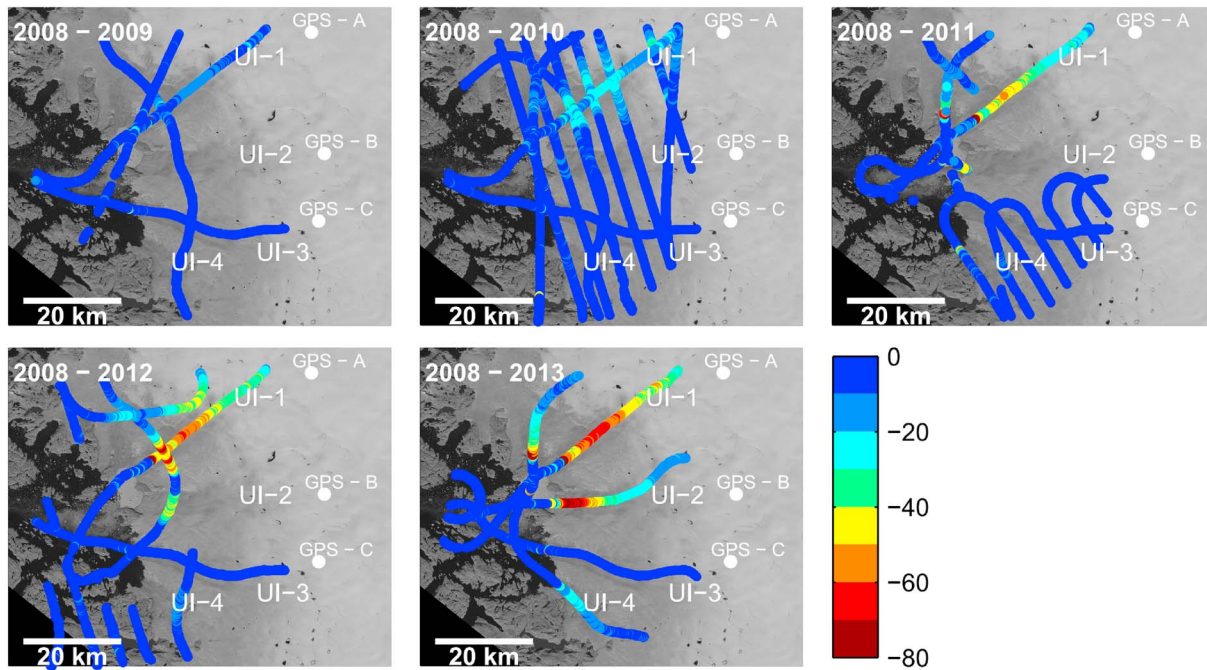
**Figure 11.** Total elevation change between the SPOT 5 HRS DEM from June 2008 [*Korona et al.*, 2009] and ATM measurements 2009–2013. The ATM measurements were made in spring of each year and therefore represent the surface lowering from the previous year, ignoring changes in snow depth from year to year.

grounding line, we add the change in ice volume, $\Delta V$, downstream of the fluxgate. The volume change due to SMB in the area downstream of the fluxgate ($\Delta$smb) is then subtracted to isolate the dynamic mass loss, thus

$$\Delta D = \Delta F + (\Delta V - \Delta\text{smb}) \qquad (2)$$

The rate of ice volume change ($\Delta V$) is estimated using altimeter surveys from NASA's ATM flights [*Krabill*, 2013] during 2003–2012 supplemented with Ice, Cloud and land Elevation Satellite (ICESat) data GLA12 Release 34 [*Zwally et al.*, 2011] during 2003–2009. ICESat elevations have a single-shot uncertainty of $\sigma$ICESat = 0.2 m, and ATM data have an elevation uncertainty of $\sigma$ATM = 0.1 m. Our procedure for deriving ice surface elevation changes is described in detail by *Khan et al.* [2013] and is similar to the method used by others [e.g., *Ewert et al.*, 2012; *Smith et al.*, 2009; *Kjeldsen et al.*, 2013]. We use the observed ice elevation change rates to interpolate (using collocation) ice thinning values onto a regular 1 × 1 km grid. We correct for the elevation change due to firn compaction, and the density of ice $\rho_{ice}$ = 917 kg m$^{-3}$ is assumed to convert volume change to mass change. Figure 4b of *Khan et al.* [2013] suggests that the lower part of UI-1 started to thin in 2004. Hence, we assume no significant thinning in 2000–2003 and estimate the volume change ($\Delta V$) during April 2003 to April 2006, April 2006 to April 2009, and April 2009 to April 2012. The volume change due to increased melt in the area below the fluxgate, $\Delta$smb, is obtained from the SMB product from MAR. Since we are only looking at the increase in mass loss since 2000, we use the SMB anomaly compared with the mean of 1970–1999. This reference period is used since it shows no general trends in SMB (Figure 5). The MAR SMB is converted from meter water equivalent (m w.e.) to mass using a constant $\rho_{ice}$ and summed over the area below the fluxgate for the periods January 2000 to December 2005, January 2006 to December 2008, and January 2009 to December 2011.

The increased flux through the gate for a given year ($\Delta F$) is given by the difference in flux ($F$) between 2000 and the given year. $F$ is calculated by dividing the fluxgate into a number of columns, $i$, of width, $w$, and height, $h$, summing the contribution from each column, thus

$$F = \sum v_i \cdot h_i \cdot w_i \cdot \rho_{ice} \qquad (3)$$

where $v_i$ is the ice speed for the given year and column, given by the ice velocity maps presented in Figure 9. We assume that the ice flow is independent of depth, i.e., that internal deformation is insignificant compared
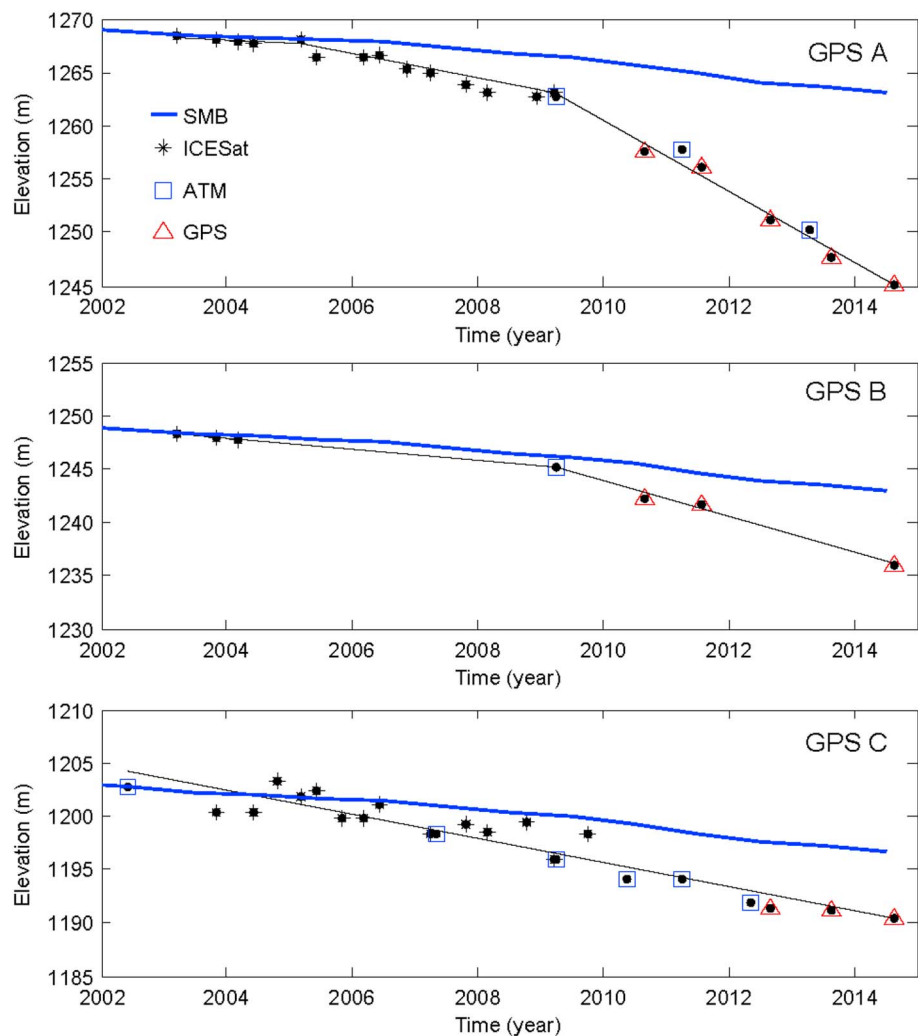
**Figure 12.** Elevation measured at the three GPS sites 30–40 km upstream; see positions in Figure 11. The elevations are extended back in time using Ice, Cloud and land Elevation Satellite (ICESat) data [*Zwally et al.*, 2011] and ATM when available. Thinning rates in m yr$^{-1}$ for GPS-A: $-0.2 \pm 0.3$ (2003–2005), $-1.3 \pm 0.2$ (2005–2009), and $-3.3 \pm 0.3$ (2009–2014). For GPS-B: $-0.5 \pm 0.3$ (2003–2009) and $-1.7 \pm 0.3$ (2009–2014). For GPS-C: $-1.1 \pm 0.1$ (2002–2014).

to the basal sliding velocity. This is a valid assumption in areas with high ice speed since they are dominated by sliding or basal till deformation [*Cuffey and Paterson*, 2011]. The ice height, *h*, is given by the difference in bed elevation from the CReSIS depth radar data and surface elevation. The bed elevation is kept constant with an uncertainty of $\pm 7.09$ m, obtained from a crossover analysis of all radar depth lines in 2009 and 2010 on the northwest coast of Greenland (L3 radar depth sounder data) [*Gogineni*, 2012]. Between 2000 and 2012 there has been a significant change in surface elevation across the fluxgate. We use the elevation change rates and uncertainties, as given in the calculations of $\Delta V$, to obtain the surface elevation. In order to obtain an estimate of *F* for the period 2000–2005 where only sparse velocity data are available, we assume that the acceleration between 2000 and 2005 occurred linearly. $\Delta F$ is estimated for the periods of winter 2000/2001 to winter 2005/2006, winter 2005/2006 to winter 2008/2009, and winter 2008/2009 to winter 2011/2012. We only use the change in winter velocities so that any increased dynamic mass loss due to anomalies in acceleration during summertime is neglected.

As with $\Delta$smb in equation (1), the anomaly compared to the period 1970–1999 is used, and units are converted from m w.e. to mass using $\rho_{ice}$. The annual MAR SMB is summed over the entire catchment for the periods January 2000 to December 2005, January 2006 to December 2008, and January 2009 to

**Table 1.** The Dynamic Mass Balance Anomaly for the Entire UI Catchment, Compared to 2000, Summed for Three Time Intervals[a]

| Year | $\Sigma\Delta F$ (Gt) | $\Sigma\Delta$smb (Gt) | $\Sigma\Delta V$ (Gt) | $\Sigma\Delta D$ (Gt) | $\Sigma\Delta$SMB (Gt) | $\Sigma\Delta$MB (Gt) |
|---|---|---|---|---|---|---|
| 2000–2005 | $-2.56 \pm 7.61$ | $-3.53 \pm 2.16$ | $-6.00 \pm 0.12$ | $-5.03 \pm 9.89$ | $-1.27 \pm 10.06$ | $-6.30 \pm 19.95$[b] |
| 2006–2008 | $-9.38 \pm 2.58$ | $-2.71 \pm 1.08$ | $-8.91 \pm 0.12$ | $-15.58 \pm 3.78$ | $-9.69 \pm 10.06$ | $-25.27 \pm 13.84$[c] |
| 2009–2011 | $-20.72 \pm 2.70$ | $-2.70 \pm 1.08$ | $-8.49 \pm 0.12$ | $-26.51 \pm 3.90$ | $-12.29 \pm 13.41$ | $-38.80 \pm 17.31$[d] |

[a]The intervals are from the beginning of the first year to the end of the last year. The catchment is shown in Figure 1.
[b]$-1.05 \pm 3.33$ Gt yr$^{-1}$.
[c]$-8.42 \pm 4.61$ Gt yr$^{-1}$.
[d]$-12.93 \pm 5.77$ Gt yr$^{-1}$.

December 2011. The modeled SMB from MAR have uncertainties of around 40 cm water equivalent (w.e.) in the ablation zone and 5 cm w.e. in the accumulation zone [*Colgan et al.*, 2015].

The results, presented in Table 1, show that the increase in dynamic mass loss is responsible for about 80% of the changes in 2000–2005 (including both years), 62% in 2006–2008, and 68% in 2009–2011. While the dynamic mass loss is thus the dominant cause of mass loss, $\Delta$SMB and $\Delta D$ increase at comparable rates over the three periods. Table 2 shows the change in flux through the fluxgate of each individual glacier. The gates are divided at the point with the lowest velocity between the glaciers; UI-3 and UI-4 could not be separated due to the location of the gate. Table 1 shows that UI-1 was the main contributor to flux changes between 2000 and 2008. In 2009–2011 UI-2 flux increases and contributes with about 15% of the total flux increase.

## 4. Discussion

Although dynamic changes in ice streams may occur due to internal switching [*Brinkerhoff and Johnson*, 2015], we find that external forcing mechanisms are more likely for a topographically constrained setting like UI. This external forcing may be due to atmospheric changes or changes in the ocean water masses arriving at the marine-terminating front of UI. Atmospheric changes can be assumed to be equal to all the four glaciers included in this study due to their mutual proximity and similar orientation. According to the bathymetry measurements [*Andresen et al.*, 2014], it is likely that the ocean water arrive through the same >1 km deep fjord to the fronts of UI-1, UI-2, and UI-3 (Figure 3), while UI-4 terminates in shallow waters, and therefore, it is not subject to the same oceanic forcing. Atmospheric changes causing an increase in surface melt may influence the ice dynamics in a variety of ways, apart from the direct dynamic consequences of ice sheet thinning. Indirect effects of surface melt may, for example, arise by increasing the basal water pressure under the ice stream [*Iken et al.*, 1993], through meltwater releasing heat to the ice at depth [*Phillips et al.*, 2010, 2013; *Meierbachtol et al.*, 2015], by enhancing calving through hydrofracturing [*Benn et al.*, 2007] or by forcing convection at the ice-ocean boundary when the meltwater is released in the fjord at depth as buoyant plumes leading to enhanced melt and undercutting at the glacier front [*Straneo et al.*, 2013; *Jenkins*, 2011]. The melting at the ice-ocean interface due to forced convection depends on the ocean temperature as well as the run-off volume and the slope of the ice ocean interface [*Jenkins*, 2011]. Changes in the water masses arriving at the marine-terminating glaciers will alter the submarine rate of melting directly and indirectly by its influence on forced convection at the ice-ocean boundary. We suggest that the asynchronous dynamic response to these essentially synchronous external forcing mechanisms is related primarily to differences in sensitivity between the glaciers due to their bedrock geometry and the proximal fjord bathymetry.

**Table 2.** $\Sigma\Delta F$ (Gt) for the Individual Glaciers[a]

| Year | UI-1 | UI-2 | UI-3 and UI-4 |
|---|---|---|---|
| 2000–2005 | $-2.84 \pm 3.21$ | $-0.24 \pm 1.85$ | $0.42 \pm 2.34$ |
| 2006–2008 | $-9.43 \pm 1.20$ | $-0.41 \pm 0.55$ | $0.44 \pm 0.77$ |
| 2009–2011 | $-18.40 \pm 1.44$ | $-3.25 \pm 0.57$ | $0.83 \pm 0.64$ |

[a]$\Sigma\Delta F$ is the change in ice flux through the fluxgate since 2000 summed over the three time intervals. The intervals are from the beginning of the first year to the end of the last year.

Three of the glaciers at UI (UI-1, UI-2 and UI-3) were flowing at similar and relatively constant speeds between 1992 and 2005. Over the period between 2006 and 2008 the total dynamic mass loss of UI increased by almost a factor of 3 compared to the dynamic mass loss between 2000 and 2005. The 2006–2008 increase

was driven primarily by the acceleration, thinning, and retreat of UI-1. UI-2 started to accelerate and thin in 2009. This, combined with continuing acceleration at UI-1, increased the dynamic mass loss contribution of UI by 65% from around 8.4 Gt yr$^{-1}$ between 2006 and 2008 to around 12.9 Gt yr$^{-1}$ between 2009 and 2011. The acceleration of the glaciers over the period 2005–2013 coincided with a period of increased mass loss from surface melt. The ratio of mass lost by increased surface melt (20–40%) to increased ice discharge (60–80%) remained about the same for the whole UI catchment. Only UI-1 and UI-2 showed major changes in dynamic behavior during the period 2000 to 2013, and their responses occurred asynchronously.

The main acceleration of UI-1 happened between 2007 and 2008. The calving front retreated rapidly during these years (Figure 6) suggesting that the acceleration is due to the breakup of a floating ice tongue of about 4 km in length. To understand the mechanisms behind the retreat of UI-1, we need to establish whether the glacier already had a floating tongue in the years before the retreat or if it reached floatation just before the disintegration. The glacier tongue was determined to be floating between 2001 and 2007 by *Enderlin and Howat* [2013] due to the significant change in slope around the area where UI-1 is grounded today. *Enderlin and Howat* [2013] found submarine melt rates generally increasing from around 1.5 m d$^{-1}$ during the melt season in 2001 to around 2 m d$^{-1}$ in 2006. Evidence for the glacier tongue being floating since 1985 until the breakup in 2007–2008 can be found in the crevasse pattern observed on the Landsat images from, e.g., 13 September 1985 and 19 September 2001 showing a clear change in the crevasse pattern at the current grounding line as well as tabular icebergs floating away from the calving front. However, surface elevation profiles in *McFadden et al.* [2011] show a sloping surface of the tongue, around 70 m elevation rise in 3 km, indicating that the tongue was not freely floating. One possible interpretation of this is that the glacier is resting on a shallow shoal, in which case UI-1 would reach floatation as a result of surface-induced thinning just before the breakup in 2007–2008. A second interpretation that we find more convincing in light of the evidence provided by the Landsat imagery is that the high surface slope was instead due to lateral friction in the narrow trough.

Investigations show the calving front started to retreat around 1998, coinciding with observations of a sudden warming of the subsurface ocean waters along the entire west coast of Greenland [*Holland et al.*, 2008]. A floating ice tongue is more sensitive to changes in ocean temperatures compared to a grounded vertical calving front, due to the large surface area in contact with ocean water [*Straneo et al.*, 2013]. Since there were no trends toward unusually high surface melt rates in the late 1990s (Figure 5), we suggest that the initialization of the retreat of UI-1, which led to the disintegration in 2006 and 2007, was due to submarine thinning caused by increased ocean temperatures in the late 1990s. Thinning of a floating ice tongue will cause a reduction in lateral shear and an increase in crevassing and calving will happen more readily [*Nick et al.*, 2010]; these processes will cause retreat and acceleration. As the calving front of UI-1 retreated in the beginning of the 2000s, it moved into a wider fjord (Figure 6). This caused divergence of the ice flow, effectively thinning the terminus, decreasing the lateral drag and increasing crevassing, that is likely to take larger sections of the terminus closer to buoyancy, thus promoting calving and terminus retreat. Furthermore, during the last decade surface melting has increased (Figure 5) leading to thinning of the ice sheet in general from around 2002/2003. Both these processes are likely to have enhanced the retreat rate leading to the disintegration of the floating ice tongue. The disintegration of the floating tongue caused a period of retreat, acceleration, and dynamic thinning lasting at least until 2010. Between July and August 2010, UI-1 accelerated again, coinciding with increased thinning rates but no significant change in the calving front position. We speculate that in July 2010 the glacier had retreated due to the continued dynamically induced thinning and reached a topographical threshold which stabilized the front position. However, the bed topography data do not reveal enough detail to substantiate this. After 2011, UI-1 has been stable with no major changes in ice flow velocity and terminus position. In 2013 the calving front is believed to have been close to vertical and grounded (Figure 2), and therefore, changes that occurred after 2010 where the front reached a stable position are likely to be less sensitive to ocean temperatures. The acceleration event in 2010 is therefore believed to be unrelated to changes in ocean temperatures. If thinning rates persist, the glacier may retreat farther inland into a wider fjord (Figure 2) which could cause further thinning and retreat.

The gradual acceleration of UI-2, and the fact that it did not start to retreat before 2008, stands in contrast to the early retreat and stepwise acceleration of UI-1. The fluctuations of the calving front position observed in the late 1990s suggest that UI-2 was also affected by the change in ocean temperatures. However, the glacier remained stable compared to UI-1. This is believed to be due to the stable position of the calving front in a narrow fjord. The retreat of UI-2 started in 2008 or 2009 after a period of 5 years with unusually high surface

melt rates (Figure 5). As UI-2 is relatively shallow, approximately 500 m near the calving front and likely to be close to or at floatation (see Figure 2), we expect that further thinning would lead to glacier acceleration due to loss of friction at the bed as well as the increase in driving stress from the steeper surface slope. The glacier is furthermore retreating inland on a reverse sloping bed and into a widening fjord, suggesting a significant potential for further retreat.

UI-3 showed a slight deceleration throughout the period 2000 to 2013 and the absence of any acceleration, thinning or retreat is noteworthy. At the glacier terminus we believe that a shallow point in the fjord is causing large icebergs to run aground. This is likely to prevent the glacier from calving freely and causes a back stress that stabilizes the glacier front, which in turn stabilizes the upstream flow. However, as Figures 2 and 3 show, UI-3 is located in a deep and long trough and further thinning will at some point bring the glacier close to floatation, and there is therefore a potential for UI-3 to retreat much farther inland than the other glaciers.

Glacier UI-4 is quite different from the other glaciers as it is shallow (less than 200 m below sea level) and flowing with relatively slow velocities below 1 km yr$^{-1}$. From 1985 to 1991 the calving front rapidly retreated along with the entire ice margin of between UI-3 and UI-4 (Figure 6). From *Andresen et al.* [2014] we know that the glacier has been continuously retreating since 1849, and so the retreat event in the late 1980s is believed to be a response to the removal of back stress due to retreat from a pinning point on the south side of the glacier. UI-4 has continuously been retreating inland since then and showed clear and large seasonal variability in the period 2009–2013. The seasonal velocity pattern of speedup in spring and slowdown during midsummer (type 3 according to *Moon et al.* [2014]) is indicating that an efficient drainage system develops at the glacier bed every year, causing it to slow down. Increased meltwater could in this aspect have a slowing effect on UI-4 since the seasonal slowdown would occur earlier when more meltwater is available. UI-4 is located in a shallow trough, in contrast to the deep troughs at the other UI glaciers, and if the gradual retreat continues, it will eventually lose contact with the ocean and become land terminating.

## 5. Conclusion

Dynamically induced mass loss tripled between the periods 2000–2005 and 2006–2008 followed by an increase of by more than 50% between the periods 2006–2008 and 2009–2011. The early increase in dynamic mass loss is attributed to the acceleration of UI-1, and the later increase is due to the acceleration of UI-2. Calculations of the partitioned increase in mass loss between 2000 and 2012 show that dynamic mass loss is the main cause of mass loss. However, the ratio between the mass lost by surface melt and that lost through ice discharge remained constant. While the increase in mass loss due to surface melt is expected to be equally spread over the four glaciers, the rapid increase in ice discharge is occurring only on two of the four outlets of UI, UI-1, and UI-2.

The different dynamic reactions of the four glaciers to similar climate forcings can be understood when looking into the detailed geometry of each individual glacier. UI-1 is the main contributor to the increased ice discharge due to the disintegration of the glaciers' floating ice tongue. The initial retreat of UI-1 is believed to be caused by warming of deeper ocean waters in the late 1990s. Furthermore, feedback mechanisms related to the width of the calving front played an important role in the retreat of the glacier. In 2009 UI-2 started to accelerate and retreat and showed dynamically induced thinning. The acceleration of the glacier may have been amplified by the positive feedback mechanism as the calving front retreated into deeper water. There is a notable absence of any changes in UI-3 as the glacier is believed to have been stabilized by a grounding point near the calving front. Finally, UI-4 showed thinning and slowing down which is mainly due to increased surface melt. At UI-1, UI-2, and UI-3 there is a potential for further destabilization should the glaciers continue to thin due to upstream widening of the troughs and their fronts being close to floatation.

## References

Andresen, C. S., K. K. Kjeldsen, B. Harden, N. Nørgaard-Pedersen, and K. H. Kjær (2014), Outlet glacier dynamics and bathymetry at Upernavik Isstrøm and Upernavik Isfjord, North-West Greenland, *Geol. Surv. Den. Greenl. Bull.*, *31*, 81–84.

Benn, D. I., C. R. Warren, and R. H. Mottram (2007), Calving processes and the dynamics of calving glaciers, *Earth Sci. Rev.*, *82*, 143–179, doi:10.1016/j.earscirev.2007.02.002.

Brinkerhoff, D. J., and J. V. Johnson (2015), Dynamics of thermally induced ice streams simulated with a higher-order flow model, *J. Geophys. Res. Earth Surf.*, *120*, 1743–1770, doi:10.1002/2015JF003499.

Carr, J. R., A. Vieli, and C. Stokes (2013), Influence of sea ice decline, atmospheric warming, and glacier width on marine-terminating outlet glacier behavior in northwest Greenland at seasonal to interannual timescales, *J. Geophys. Res. Earth Surf.*, *118*, 1210–1226, doi:10.1002/jgrf.20088.

Citterio, M., and A. P. Ahlstrøm (2013), Brief communication 'The aerophotogrammetric map of Greenland ice masses', *Cryosphere*, *7*, 445–449, doi:10.5194/tc-7-445-2013.

Colgan, W., J. Box, M. Andersen, X. Fettweis, B. Csatho, R. Fausto, D. van As, and J. Wahr (2015), Greenland high elevation mass balance: Inference and implication of reference period (1961–1990) imbalance, *Ann. Glaciol.*, *70*, 105–117.

Cuffey, K. M., and W. S. B. Paterson (2011), *The Physics of Glaciers,* 4th ed., Elsevier, Oxford.

Enderlin, E. M., and I. M. Howat (2013), Submarine melt rate estimates for floating termini of Greenland outlet glaciers (2000–2010), *J. Glaciol.*, *59*(213), 67–75, doi:10.3189/2013JoG12J049.

Enderlin, E. M., I. M. Howat, and A. Vieli (2013), High sensitivity of tidewater outlet glacier dynamics to shape, *Cryosphere*, *7*, 1007–1015, doi:10.5194/tc-7-1007-2013.

Enderlin, E. M., I. M. Howat, S. Jeong, M.-J. Noh, J. H. van Angelen, and M. R. van den Broecke (2014), An improved mass budget for the Greenland ice sheet, *Geophys. Re. Lett.*, *41*, 866–872, doi:10.1002/2013GL059010.

Ewert, H., A. Groh, and R. Dietrich (2012), Volume and mass changes of the Greenland ice sheet inferred from ICESat 203 and GRACE, *J. Geodyn.*, *59–60*, 11–123, doi:10.1016/j.jog.2011.06.003.

Fettweis, X., B. Franco, M. Tedesco, J. H. van Angelen, J. T. M. Lenaerts, M. R. van den Broeke, and H. Gallée (2013), Estimating the Greenland ice sheet surface mass balance contribution to future sea level rise using the regional atmospheric climate model MAR, *Cryosphere*, *7*, 469–489, doi:10.5194/tc-7-469-2013.

Gogineni, P. (2012), *CReSIS Radar Depth Sounder L2 Data*, Lawrence, Kansas, USA, Digital Media. [Available at http://data.cresis.ku.edu/.]

Helm, V., A. Humbert, and H. Miller (2014), Elevation and elevation change of Greenland and Antarctica derived from CryoSat-2, *Cryosphere*, *8*, 1539–1559, doi:10.5194/tc-8-1539-2014.

Holland, D. M., R. H. Thomas, B. de Young, M. H. Ribergaard, and B. Lyberth (2008), Acceleration of Jakobshavn Isbræ triggered by warm subsurface ocean waters, *Nat. Geosci.*, *1*(10), 659–664, doi:10.1038/ngeo316.

Iken, A., K. A. Echelmeyer, W. Harrison, and M. Funk (1993), Mechanisms of fast flow in Jakobshavns Isbræ, West Greenland: Part I. Measurements of temperature and water level in deep boreholes, *J. Glaciol.*, *39*(131), 15–25.

Jenkins, A. (2011), Convection-driven melting near the grounding lines of ice shelves and tidewater glaciers, *J. Phys. Oceanogr.*, *41*(12), 2279–2294, doi:10.1175/JPO-D-11-03.1.

Joughin, I., B. Smith, I. Howat, and T. Scambos (2010), *MEaSUREs Greenland Ice Sheet Velocity Map From InSAR Data. [Subset Used: Upernavik Area]*, Natl. Snow and Ice Data Cent., Boulder, Colo. [Available at http://dx.doi.org/10.5067/MEASURES/CRYOSPHERE/nsidc-0478.001.]

Joughin, I., B. Smith, I. Howat, and T. Scambos (2011), *MEaSUREs Greenland Ice Velocity: Selected Glacier Site Velocity Maps From InSAR. [Upernavik, W72.90N]*, NASA National Snow and Ice Data Center Distributed Active Archive Center, Boulder, Colo. [Available at http://dx.doi.org/10.5067/MEASURES/CRYOSPHERE/nsidc-0481.001.]

Khan, S. A., et al. (2013), Recurring dynamically induced thinning during 1985 to 2010 on Upernavik Isstrøm, West Greenland, *J. Geophys. Res. Earth Surf.*, *118*, 111–121, doi:10.0129/2012JF002481.

Khan, S. A., et al. (2014a), Sustained mass loss of the northeast Greenland ice sheet triggered by regional warming, *Nat. Clim. Change*, *4*, 292–299, doi:1038/nclimate2161.

Khan, S. A., et al. (2014b), Glacier dynamics at Helheim and Kangerdlugssuaq glaciers, southeast Greenland, since the Little Ice Age, *Cryosphere*, *8*, 1497–1507, doi:10.5194/tc-8-1497-2014.

Khan, S. A., A. Aschwanden, A. A. Bjørk, J. Wahr, K. K. Kjeldsen, and K. H. Kjær (2015), Greenland ice sheet mass balance: A review, *Rep. Prog. Phys.*, *78*, 046801, doi:10.1088/0034-4885/78/4/046801.

Kjeldsen, K. K., S. A. Khan, J. Wahr, N. J. Korsgaard, K. H. Kjær, A. A. Bjørk, R. Hurkmans, M. R. van den Broeke, J. L. Bamber, and J. H. van Angelen (2013), Improved ice loss estimate of the northwestern Greenland ice sheet, *J. Geophys. Res. Solid Earth*, *118*, 698–708, doi:10.1029/2012JB009684.

Korona, J., E. Berthier, M. Bernard, F. Rmy, and E. Thouvenot (2009), SPIRIT. SPOT 5 stereoscopic survey of polar ice: Reference images and topographies during the fourth international polar year (2007–2009), *ISPRS J. Photogramm. Remote Sens.*, *64*(2), 204–212.

Krabill, W. B. (2013), *IceBridge ATM L2 Icessn Elevation, Slope, and Roughness, [1993-2012]*, NASA Distributed Active Archive Center at the National Snow and Ice Data Center, Boulder, Colo., Digital media. [Available at http://nsidc.org/data/ilatm2.html.](2012).

Lea, J. M., D. W. F. Mair, and B. R. Rea (2014), Evaluation of existing and new methods for tracking glacier terminus change, *J. Glaciol.*, *60*, 323–332, doi:10.3189/2014JoG13J061.

McFadden, E. M., I. M. Howat, I. Joughin, B. E. Smith, and Y. Ahn (2011), Changes in the dynamics of marine terminating outlet glaciers in west Greenland (2000–2009), *J. Geophys. Res.*, *116*, F02022, doi:10.1029/2010JF001757.

Meier, M. F., and A. Post (1987), Fast tidewater glaciers, *J. Geophys. Res.*, *92*(B9), 905–9058.

Meierbachtol, T. W., J. T. Harper, N. F. Humphrey, and D. J. Brinkerhoff (2015), Thermal boundary conditions on western Greenland: Observational constraints and impacts on the modeled thermomechanical state, *J. Geophys. Res. Earth Surf.*, *120*, 623–636, doi:10.1002/2014JF003375.

Moon, T., and I. Joughin (2008), Changes in ice front position on Greenland's outlet glaciers from 1992 to 2007, *J. Geophys. Res.*, *113*, F02022, doi:10.1029/2007JF000927.

Moon, T., I. Joughin, B. Smith, M. R. van den Broecke, W. J. van de Berg, B. Noël, and M. Usher (2014), Distinct patterns of seasonal Greenland glacier velocity, *Geophys. Res. Lett.*, *41*, 7209–7216, doi:10.1002/2014GL061836.

Morlighem, M., E. Rignot, J. Mouginot, H. Seroussi, and E. Larour (2014), Deeply incised submarine glacial valleys beneath the Greenland ice sheet, *Nat. Geosci.*, *7*, 418–422, doi:10.1038/NGEO2167. Advanced online publication 18 May 2014.

Nick, F. M., A. Vieli, I. M. Howat, and I. Joughin (2009), Large-scale changes in Greenland outlet glacier dynamics triggered at the terminus, *Nat. Geosci.*, *2*, 110–114, doi:10.1038/NGEO394.

Nick, F. M., C. J. Van der Veen, A. Vieli, and D. I. Benn (2010), A physically based calving model applied to marine outlet glaciers and implications for the glacier dynamics, *J. Glaciol.*, *56*(199), 781–794, doi:10.3189/002214310794457344.

Nielsen, K., S. A. Khan, N. J. Korsgaard, K. H. Kjær, J. Whar, M. Bevis, L. A. Sterns, and L. H. Timm (2012), Crustal uplift due to ice mass variability on Upernavik Isstrøm, west Greenland, *Earth Planet. Sci. Lett.*, *353–354*, 182–189, doi:20.1016/j.epsl.2012.08.024.

Phillips, T., H. Rajaram, and K. Steffen (2010), Cryo-hydrologic warming: A potential mechanism for rapid thermal response of ice sheets, *Geophys. Res. Lett.*, *37*, L20503, doi:10.1029/2010GL044397.

Phillips, T., H. Rajaram, W. Colgan, K. Steffen, and W. Abdalati (2013), Evaluation of cryo-hydrologic warming as an explanation for increased ice velocities in the wet snow zone, Sermeq Avannarleq, West Greenland, *J. Geophys. Res. Earth Surf.*, *118*, 1241–1256, doi:10.1002/jgrf.20079.

Schoof, C. (2007), Ice sheet grounding line dynamics: Steady states, stability, and hysteresis, *J. Geophys. Res.*, *112*, F03S28, doi:10.1029/2006JF000664.

Smith, B. E., H. A. Fricker, I. R. Joughin, and S. Tulaczyk (2009), An inventory of active subglacial lakes in Antarctica detected by ICESat (2003-2008), *J. Glaciol.*, *55*, 573–595, doi:10.3189/002214309789470879.

Straneo, F., and P. Heimbach (2013), North Atlantic warming and the retreat of Greenland's outlet glaciers, *Nature*, *504*, 36–43, doi:10.1038/nature12854.

Straneo, F., et al. (2013), Challenges to understanding the dynamic response of Greenland's marine terminating glaciers to oceanic and atmospheric forcing, *Bull. Am. Meteorol. Soc.*, *94*, 1131–1144, doi:10.1175/BAMS-D-12-00100.1.

The European Space Agency Climate Change Initiative - Ice Sheets program for Greenland (ESA cci) (2015), http://products.esa-icesheets-cci.org/products/.

van den Broeke, M., J. Bamber, J. Ettema, E. Rignot, E. Schrama, W. J. van de Berg, E. van Meijgaard, I. Velicogna, and B. Wouters (2009), Partitioning recent Greenland mass loss, *Science*, *326*, 984–986.

Weidick, A. (1958), Frontal variations at Upernaviks Isstrø m in the last 100 years, *Medd. Dan. Geol. Forening*, *14*, 52–60.

Zwally, H. J., R. Schutz, C. Bentley, J. Bufton, T. Herring, J. Minster, J. Spinhirne, and R. Thomas (2011), *GLAS/ICESat L2 Antarctic and Greenland Ice Sheet Altimetry Data V031*, NASA Distributed Active Archive Center at the National Snow and Ice Data Center, Digital media, Boulder, Colo.